

# Models and Mechanisms of the Morphogenesis of Biological Structures

Technical Report UT-CS-11-681

Kristy S. Van Hornweder<sup>\*</sup>

Department of Electrical Engineering & Computer Science  
University of Tennessee, Knoxville  
kvanhorn@utk.edu

September 27, 2011

## Abstract

This report presents a discussion and illustration of mathematical and conceptual models of the morphogenesis of several biological structures. These biological structures serve useful purposes in organisms and they include branching structures, tubes, limbs, follicles and bristles, sheets and layers, and segments and somites. The analysis of the mathematical models includes a conceptual description of the mechanism behind the algorithm and numerous illustrative examples, which are often accompanied by equations and examples of the effects of varying a parameter in the system. Also addressed is the idea that a clearer understanding of the development of biological structures will lead future researchers to build artificial nanorobotic structures with a much higher level of complexity and sophistication than the current macroscale robots.

---

<sup>\*</sup> This report may be used for any non-profit purpose provided that the source is credited.

# 1 Introduction

Nanotechnology and nanorobotics are exciting areas of research in the computing world. Of great interest is to obtain the ability to build artificial structures beginning at the molecular level as opposed to the current approach of beginning from the macroscale level. Construction beginning from the molecular level would allow much more fine-tuned and sophisticated structures to be assembled. Many of these artificial machines would have the capacity of self maintenance and self repair, as would be a necessity for a robot exploring a distant planet, for example. Researchers strongly believe that the best models for building these structures have existed in the biological world for a billion years. Nature has perfected ways to construct interesting and useful structures for a multitude of different functions in organisms. The study of morphogenesis and biological development may very well pave the way for the future of robotics and nanotechnology. This report gives a brief overview of the computational and mathematical models and mechanisms behind the development of several different biological structures, including branching structures, tubes, limbs, follicles and bristles, sheets and layers, and segmented structures and somites.

## 2 Interesting and Useful Biological Structures

### 2.1 Branching Structures

Several examples of branching structures are discussed below, including the lung airway, systems of blood vessels in the liver, capillary networks in the liver, leaf venation patterns, and general branching structures.

#### 2.1.1 Lung Airway

##### 2.1.1.1 Fractal Model

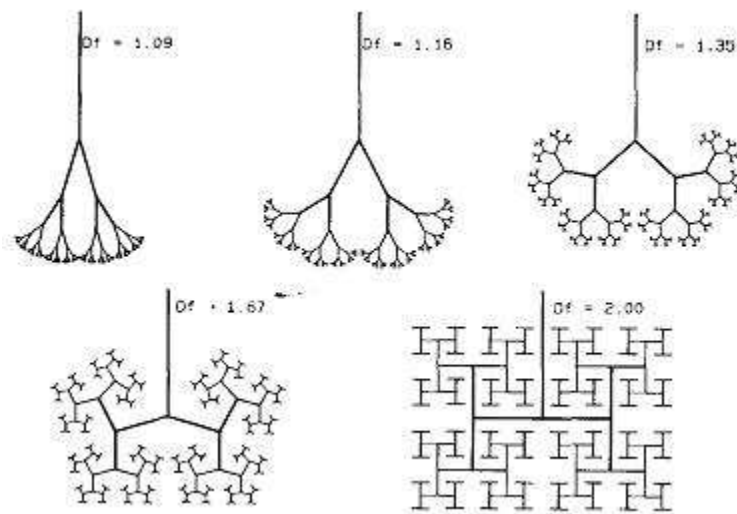
Fractal geometry is a natural choice as a mathematical model for the lung airway. Similar to fractal patterns, the lung airway is a self-similar structure over many size scales and it contains a high degree of heterogeneity. Lung airway structures are largely determined by geometrical parameters such as the length, diameter, angle, and scale of the branches. Heterogeneity results from the existence of the variation of these parameters for branches of different scales. The geometrical properties may depend on boundary constraints as well as environmental factors such as illness and injury. In addition to geometrical parameters, fluid dynamical rules [20] such as flow rate also determine the means by which branching structures develop.

The fractal model in [15] is briefly presented here as an illustrative example. The model consists of simple dichotomous branching, that is, a parent branch gives rise to two daughter branches, and the length of the daughter branches is a fixed percentage of the length of the parent branch. The measure  $D_f$  is the fractal dimension, which measures the space-filling complexity of the structure. An equation [15] for determining  $D_f$  is given by

$$1 - D_f = \frac{\log(\text{total branch length})}{\log(\text{average branch length})} = \frac{\log(rN)}{\log(r)}$$

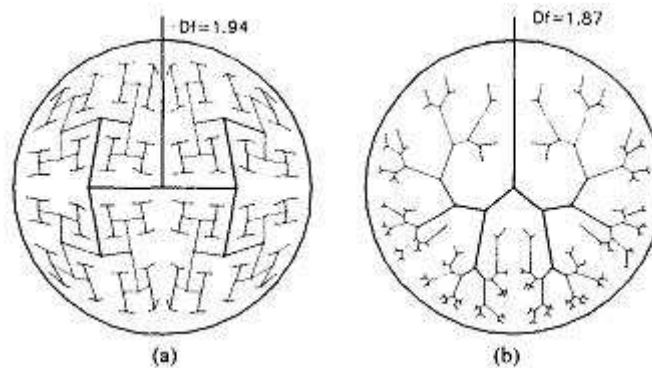
Here  $N$  indicates the number of branches formed at a branch point (in this case, 2), and  $r$  denotes the similarity ratio between parent and daughter branch. The length of a daughter branch is  $r$  times the length of its parent branch.

Figure 1 shows the different structures resulting from five values of  $r$ : 0.53, 0.55, 0.60, 0.66, and 0.71 respectively. The measure  $D_f$  is also given. The branch angle was selected to result in structures that fill the space optimally without branch overlap [15]. It is clear that larger values of  $r$  produce structures that fill more space and thus become “bushier”.



**Figure 1.** “Bushiness” of branching structures [15].

Another important factor in branch development is the existence of boundary constraints, namely, the chest wall border. In Figure 2a, a structure with a circular boundary is illustrated. At each branching step, the remaining area is successively divided in half. Many of the junctions are now “bent” in order for the branches to properly fill the constrained space.



**Figure 2.** Addition of (a) circular boundary and (b) branch angle restriction [15].

To more accurately represent the real lung airway, an angle restriction must also be imposed on the formation of the structure. Figure 2b above shows the result of limiting the range of the branch angle from 40-50 degrees for all branches. Each successive generation contains more rapid curvature, leading to the restricted space becoming more completely filled [15].

### 2.1.1.2 Mouse Lung Development

The Nature review article [12] discusses branching modes used in mouse lung development. The three branching modes are domain branching, planar bifurcation, and orthogonal bifurcation. Operations involved in branching include periodicity generator, domain specifier, bifurcator, and rotator. Each branching mode will be discussed here briefly.

In domain branching, daughter branches are formed in rows, as shown in the top portion of Figure 3. The rows can be formed in four different directions, dorsal, ventral, lateral, and medial. Two patterning systems are used in directing the branching scheme. Proximal-distal patterning includes a periodicity generator, which controls branching sequencing in each domain. Circumferential patterning determines the positions of the domains and specifies the order in which the domains will be used.

Planar branching is illustrated in the middle portion of Figure 3. The tip of a branch expands and bifurcates, forming a pair of tertiary branches, which in turn bifurcate to form four quaternary branches, all of which lie in the same plane.

Orthogonal branching also involves bifurcation at the tips, but between each round of branching, the branch is rotated 90 degrees, resulting in four tertiary branches that are arranged in a rosette pattern. This is depicted in the bottom portion of Figure 3.

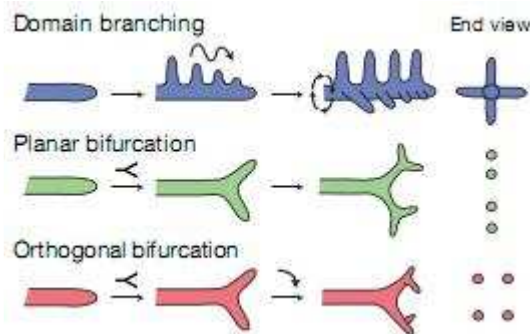


**Figure 3.** Modes of branching in lung development [12].

Domain branches are used first, and they create the supporting structure of each lobe. Planar branches form the thin edges of the lobes, and orthogonal branches build the lobe surface and fill the interior of the lobes. The organization of the three types of branching modes in a developing mouse lung are shown in Figure 4. All three branching modes can be used simultaneously. A single branch can use more than one branching mode. In different lineages, branching occurs at different rates. The branching mechanism in each lineage is executed independently; it is not controlled by a global clock. The mouse lung structure contains seven or more generations of branching. Occasionally, errors occur in the development of the branching tree. In a branch

displacement error, a branch originates from the wrong parent, and in a skipping generation error, a branch is missing. Despite these errors, branching will continue normally in subsequent generations of branches.

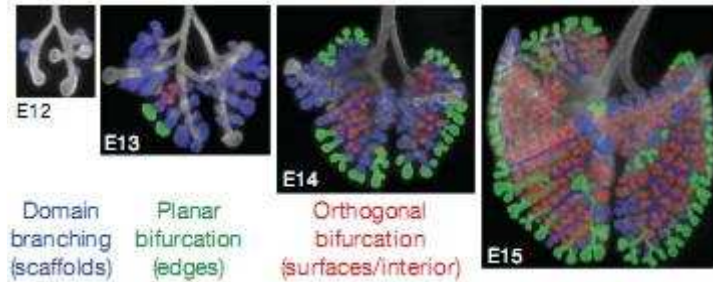


**Figure 4.** Mouse lung development using three branching modes [12].

### 2.1.1.3 Human Lung Airway

An example of a computer simulation of the human lung airway is given in Figure 5. This branching structure contains approximately 27,000 terminals, which is comparable to the real human lung [20]. Quantitative measures, such as the average diameter of the terminals and the average volume of their drainage basins are consistent with the real measurements [20].

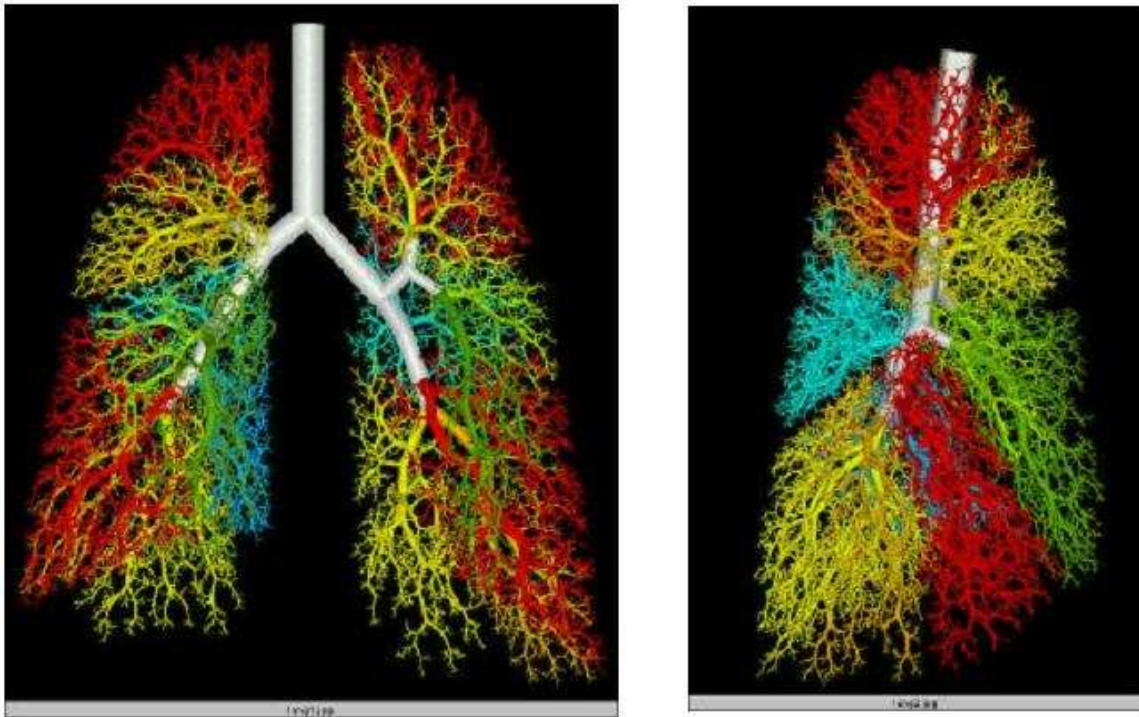


**Figure 5.** Simulation of human lung airway [20].

### 2.1.2 Blood Vessels in the Liver

Another useful application of branching structures is a system of blood vessels. Figure 6 displays an example of a computer simulation of blood vessels in the liver. The branches are constructed on a grid, which represents the liver boundary. The branches are connected using a branch extension algorithm [20] based on the vacancy of neighboring points on the grid. The system consists of inlet (arteries) and outlet (veins) vessels, and they are shown in the figure in different colors.

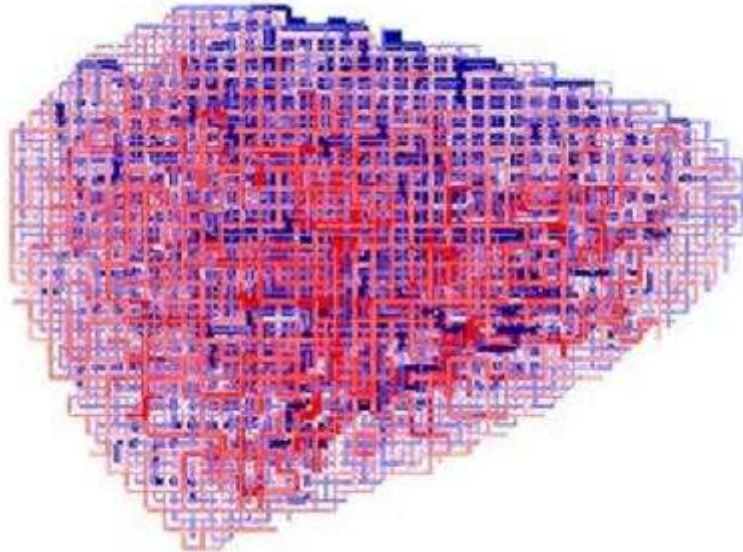


**Figure 6.** Simulation of blood vessels in the liver [20].

### 2.1.3 Capillary Network in the Liver

A third interesting example of branching structures is a capillary network. In Figure 7, a computer simulation of a capillary network in the liver is illustrated. The network is established between the inlet and outlet blood vessels, and is known as a sinusoid. A cubic grid structure is used to represent the system. The network is established by applying a branch removal algorithm [20] that determines which branches remain and which are removed based on flow rates and pressure in the capillary lines. The flow rate and pressure are depicted by the thickness and the color intensity of the lines, respectively.

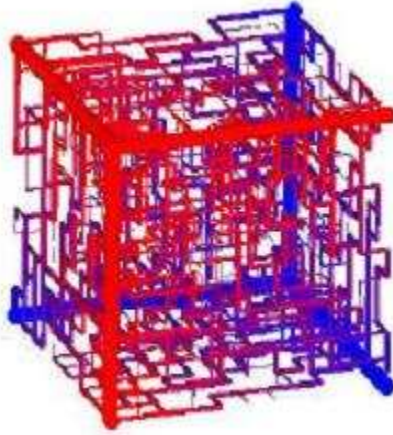


**Figure 7.** Simulation of capillary network in the liver [20].

## 2.1.4 Leaf Venation

### 2.1.4.1 Reaction-Diffusion Model

A reaction-diffusion model leads to interesting patterns that emerge from a medium that is initially homogeneous and continuous. Two or more morphogens diffuse throughout the medium and interact with one another, resulting in the formation of patterns. Partial differential equations are used to mathematically model a reaction-diffusion system. Meinhardt [11] proposed a model to construct a network structure in a homogeneous environment. Figure 8 depicts a leaf venation pattern produced by Meinhardt's model on a hexagonal grid. Four morphogens in the form of activators and inhibitors interact with each other to determine the extension of growing tips and the development of lateral branches.



**Figure 8.** Leaf venation pattern using Meinhardt's reaction-diffusion model [18].

### 2.1.4.2 Space Expansion Model

Another model of branching involves Gottlieb's geometrical model [6] in which the space expands uniformly. A grid system is used to recursively construct branches based on distance. This process is illustrated in the left portion of Figure 9. The grid is initially 2x2 cells, and new branches result from connecting grid cell centers to the structure, provided the distance between the cell center and the structure is sufficiently large [18]. The space is then scaled and each cell is divided into a smaller 2x2 grid, and the process repeats until the desired level of detail is obtained. An example of the application of this technique to leaf venation is shown in the right portion of Figure 9.

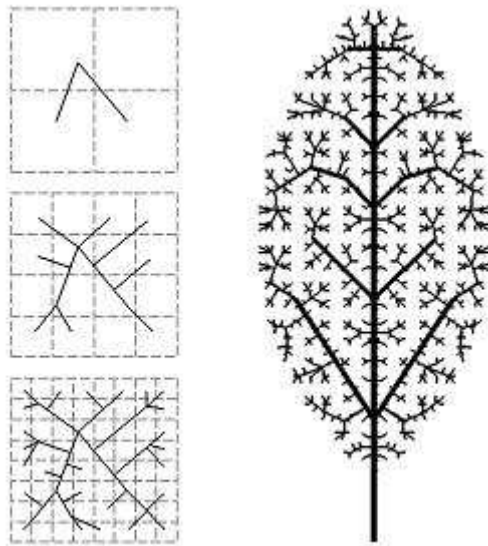


**Figure 9.** Leaf venation using Gottlieb's model of expanding space [18].

## 2.1.5 General Branching Structures

### 2.1.5.1 Cellular Automata Model

The space for cellular automata is represented by a uniform grid of cells where time is incremented in discrete steps. Each cell changes state based on its previous state and the states of its closest neighbors. An example of Maltese crosses [22] generated by the application of cellular automata is depicted in Figure 10. The structure is constructed on a square grid that begins with a single cell as the seed. The pattern spreads into neighboring cells, provided that the branches do not collide with one another.



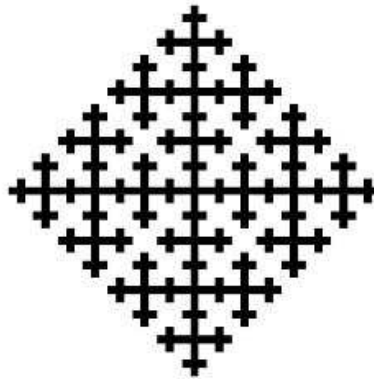


**Figure 10.** Branching structure produced by cellular automata [18].

### 2.1.5.2 *L-Systems Model*

Another mechanism for generating branching structures is L-systems, which simulate the development of such structures that are constructed from discrete modules [18]. Either context-free or context-sensitive L-systems can be used to control the development of these structures. L-systems are able to detect changes of shape in extremities or internal parts that occur during the developmental process [18]. They can also detect collisions between different branches and between branches and the environment. An example of a branching structure generated by L-systems is shown in Figure 11. An environmentally sensitive L-system [8] was used to produce this structure.

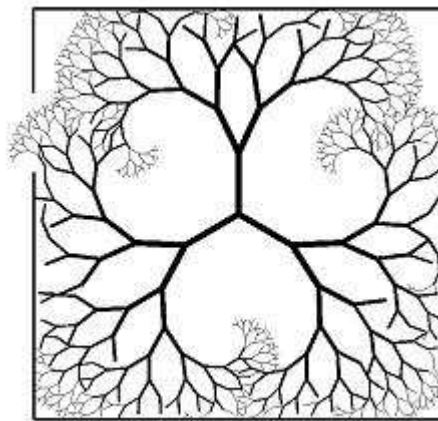


**Figure 11.** Branching structure resulting from L-systems [18].

## 2.2 Tubes

Tubes allow transportation of substances into and out of cells and tissues. Biological tube structures are useful for fluid secretion, nutrient absorption, and gas exchange. The development of tubes is dependent on factors such as cell polarity, cell proliferation, organization of intercellular junctions, invagination, lumen formation, and tube elongation. Several examples of mechanisms for tube formation are discussed below.

### 2.2.1 Sheet Folding and Invagination

One means of forming a tube structure is by the inward folding of an epithelial sheet of cells, as illustrated in Figure 12. Tubes formed in this manner appear in the vertebrate lung, liver, and neural tube, as well as *Drosophila* salivary glands and tracheal sacs [7]. The sheet of cells contains polarity in that the top is the apical end and the bottom is the basal end. The cells in the sheet elongate to become columnar. The cells proceed to become wedge-shaped while the sheet invaginates, that is, folds inward to form a channel or tube structure, as shown in the rightmost portion of the figure. The formation of this structure may involve rearrangement of the cytoskeleton, increasing cell adhesion, or changes in the extracellular matrix [7].

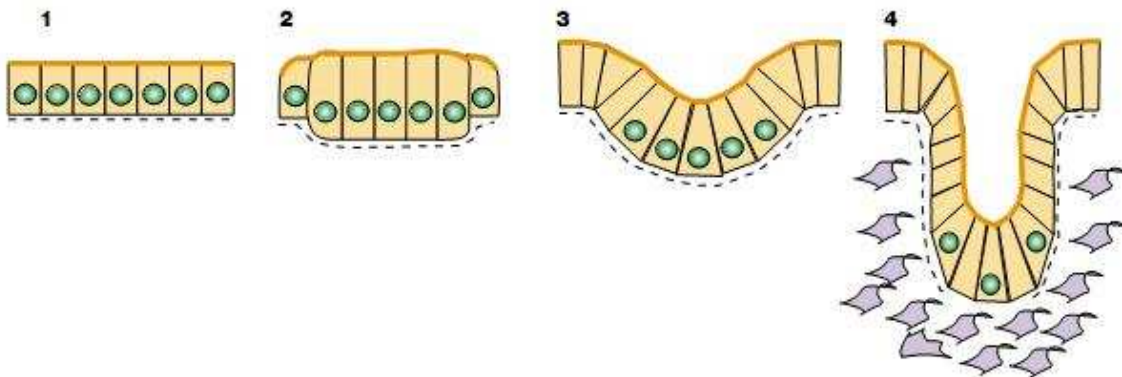


**Figure 12.** Tube formation by sheet folding [7].

The classic paper [16] discusses mechanical operations involved in the formation of tubular structures. Their model considers simple cuboidal epithelium where the cells contain microfilament bundles attached to the cell membrane in a “purse-string” configuration around the cell apex. Contraction of these fibers results in the narrowing of the cell apex, and the cell transforms from a cylindrical structure to a cone structure, as shown in Figure 13.

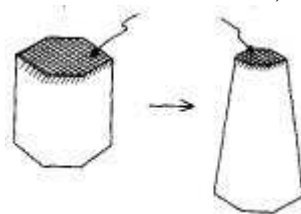


**Figure 13.** Contraction of the cell apex [16].

The contraction mechanism of the cell apex is involved in several biological functions, including invagination (as in gastrulation), exvagination, uniform and periodic thickenings (as in neural plate formation), wave propagation, and tube formation. A simulation of sea urchin gastrulation is illustrated in the left side of Figure 14. The beginning structure is a spherical configuration of a single layer of uniform-sized cells. A trigger cell contracts at its apex, which stimulates the propagation of a wave of contraction, causing the neighboring cells to also contract at their apex. This process of contraction leads to invagination of the cell layer, where the cells buckle and fold inside, creating a cavity. Further folding of cells can eventually result in the formation of a tube, as shown in the right side of Figure 14.

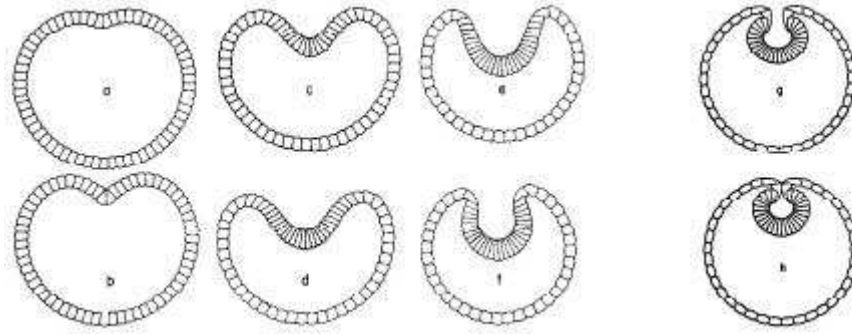


**Figure 14.** Gastrulation (left) and neurulation (all) [16].

As given in the Appendix of [16], parameters involved in tube formation include number of cells, number of active cells, cell height, cavity leakage, cavity fluid compliance, filament band trigger, viscosity, and elasticity.

### 2.2.2 Layers of Sheets

Another way epithelial sheets can form tube structures is by the alignment of layers of sheets, as displayed in Figure 15. Structures of this type appear in the formation of vein systems in insect wings. The two layers of cells actually originate from a single layer, which folds back on itself to form two layers in which the cells are aligned [7]. As shown in the figure, the cells differentiate to form future vein and intervein cells. The differentiation is based on adhesive properties of the cells.

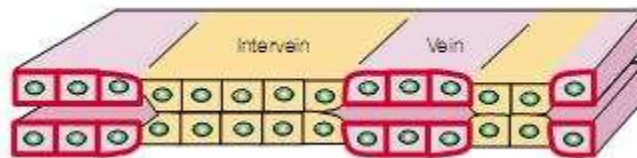


**Figure 15.** Tube formation from sheets of cells [7].

### 2.2.3 Branching

Branching tube structures can also be formed from epithelial sheets of cells, as shown in Figure 16. A biological example of this structure is the *Drosophila* tracheal system. The primary branches are two cells wide and the tubes lengthen by cell narrowing and extension [7]. The cells at the tips of the primary tubes elongate, resulting in secondary branches and terminals.

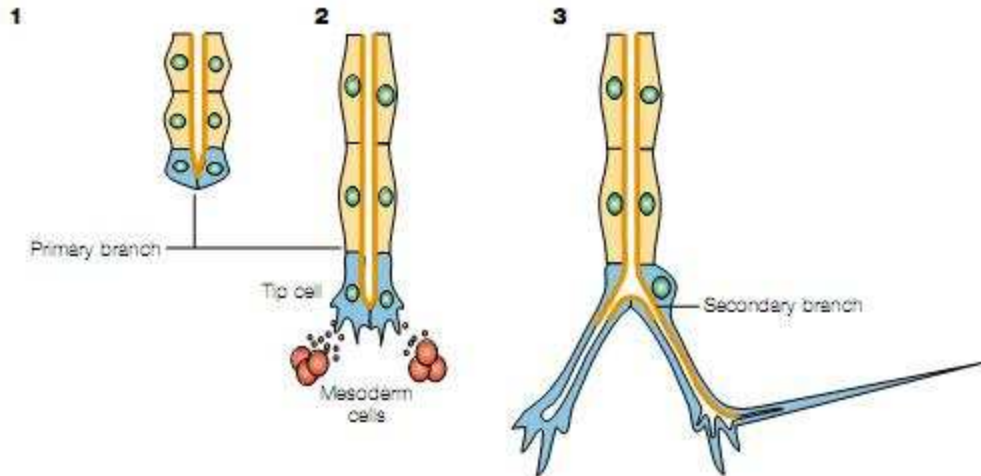


**Figure 16.** Formation of branching tube structures [7].

### 2.2.4 Budding

Tubes that arise from buds are depicted in Figure 17. Biological structures such as mammary glands, hair follicles, and the pancreas bud can be formed from a budding mechanism. The cells in these structures lack the apical-basal polarity present in the structures discussed previously. As the bud enlarges, a small lumen is formed in its interior. The bud continues to expand and several lumens are formed, which eventually coalesce into one continuous lumen.

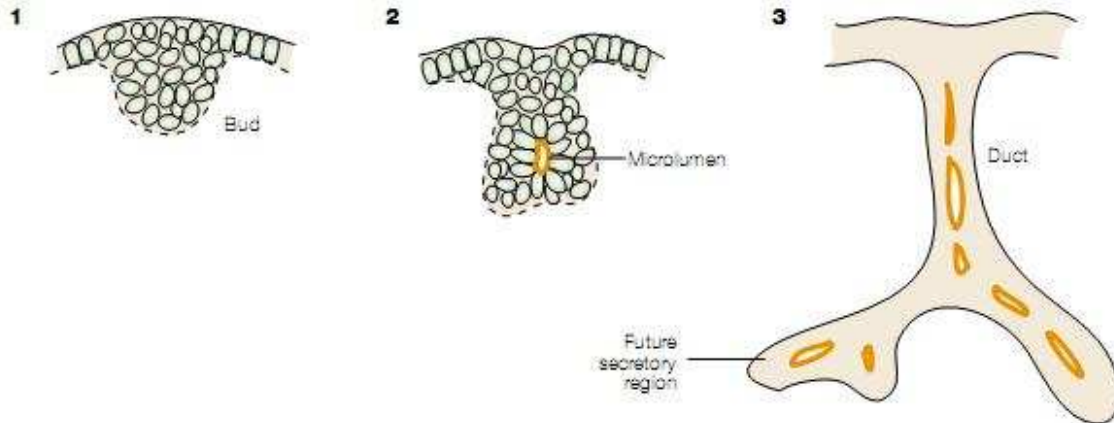


**Figure 17.** Tube formation by budding [7].

### 2.2.5 Groups of Cells

Lumen formation can result from the congregation of several cells, as shown in Figure 18. These unpolarized cells join together to form a cluster in the center of a cord. Many of these cells then become polar and junctional complexes are formed, which leads to the development of the lumen. The gut of an organism can be formed in this manner.

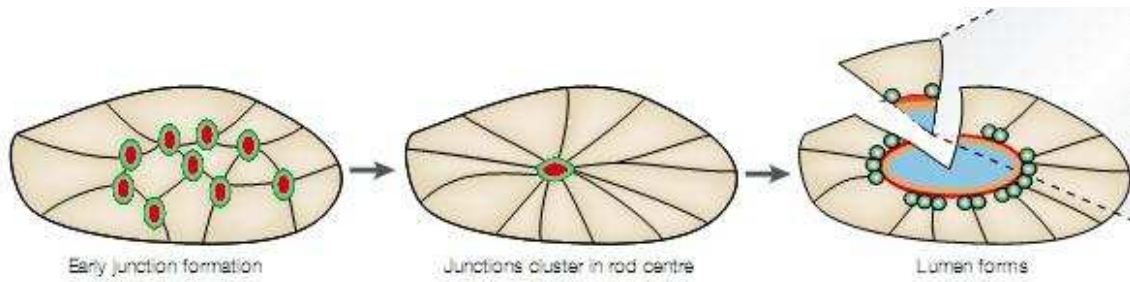


**Figure 18.** Lumen formation from a cord of cells [7].

### 2.2.6 Single Cells

A lumen can also be formed from a single elongated cell, such as that in the secondary branches of the *Drosophila* tracheal system or the *C. elegans* excretory cell. This process is illustrated in Figure 19. A channel is formed inside the cell which may have a closed end and an open end.



**Figure 19.** Lumen formation from a single cell [7].

### 2.2.7 Stacks of Aggregate Rings

The tubes in Figure 20 are constructed from sphere-shaped aggregates of cells. Each aggregate (sphere) consists of 257 cells, and 10 aggregates are placed in a circular arrangement to form a ring. As shown in the figure, these rings are stacked to form a tube structure. The rings are packed closely together so that each aggregate is adjacent to two other aggregates each above and below. This type of tube structure can represent a component of blood vessels, lungs, kidneys, and intestines [14].



**Figure 20.** Tube formation from cell aggregates [14].

### 2.2.8 Tube Joining

Another way of forming tubes, such as blood vessels, is by the joining of two existing tubes to form a single tube. This mechanism is shown in Figure 21. Lumen formation resulting from tube joining can be seen in the *Drosophila* tracheal system. A track is constructed and serves as a bridge between the two original tubes, which then proceed to move towards each other until they merge into a single tube.

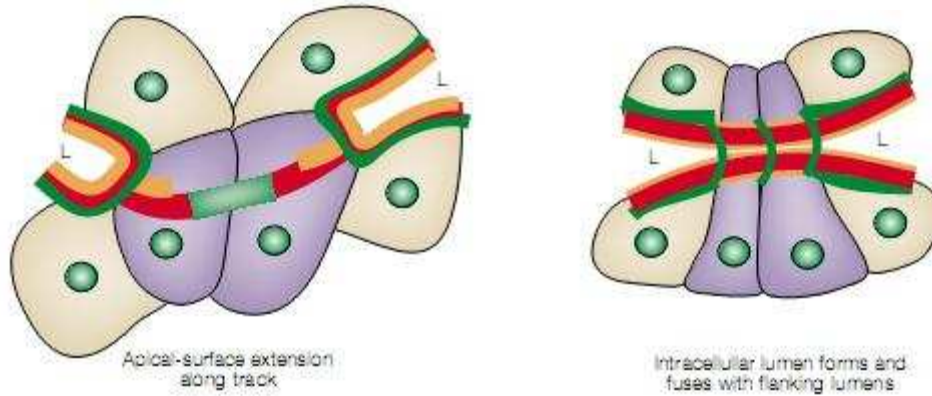


**Figure 21.** Joining of two tubes [7].

### 2.2.9 Vasculogenesis

The formation of blood vessels results from cells that assemble into a cord-like structure. Networks of cords a few cells thick are formed, which subsequently merge into larger vessels. A schematic of this process is depicted in Figure 22. The blue and red cells at the bottom migrate and are concatenated to the forming cords. Many of the cells will also merge into cords along the way. Groups of several cords coalesce into larger vessels, such as the dorsal aorta shown in part **d** of the figure.

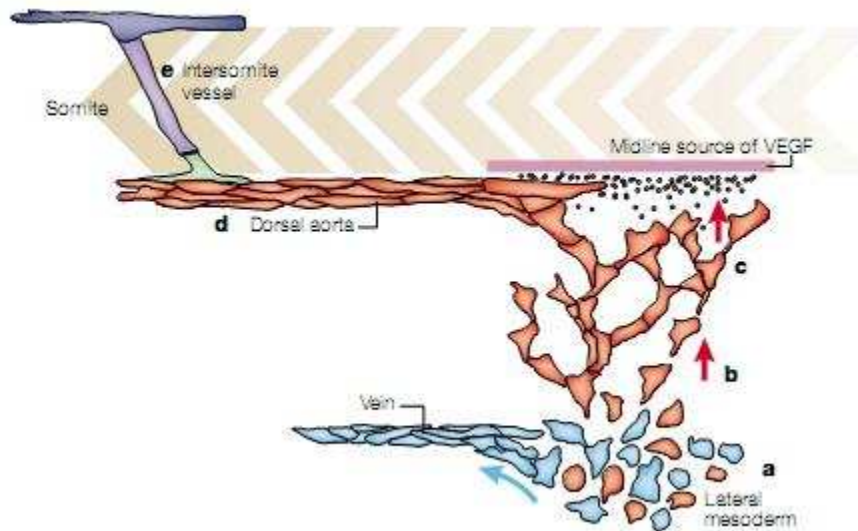


**Figure 22.** Formation of blood vessels [7].

### 2.3 Limbs

Limbs begin as homogeneous buds that develop in a thin tube structure. The early stages of limb development are illustrated in Figure 23. In part **A**, the center focus becomes a zone of recruitment to which cells are attracted to form an aggregate. The cells migrate to the focus through a process of chemotaxis. The focus is amplified autocatalytically while the cells surrounding a focus are depleted. Foci are prohibited from each other's zones of influence.

Thus, the system is controlled by a process of local activation and lateral inhibition. The limb structures form sequentially in the direction of the proximo-distal axis. In part **B** of the figure, the focus elongates, and the attraction of cells is limited to the distal end. Eventually, the foci may form a branching structure, as shown in part **C** of the figure.

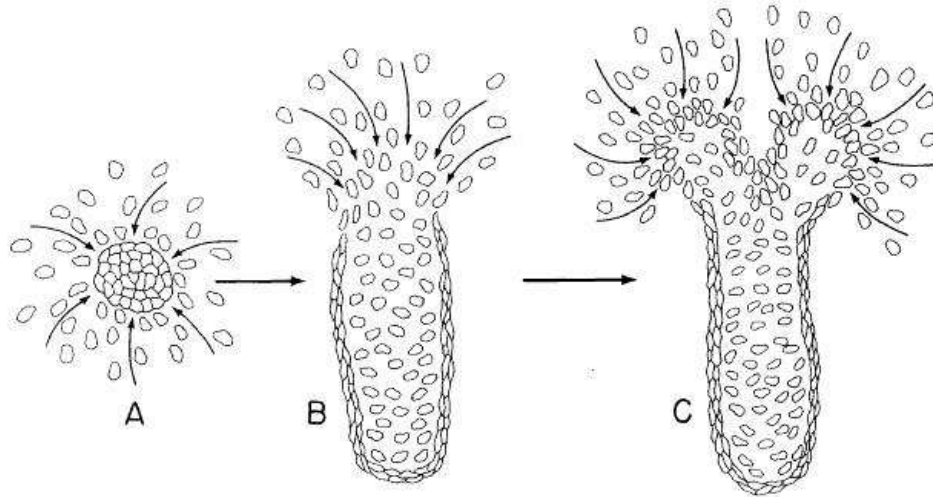


**Figure 23.** Growth and development of a limb [17].

Variations of limb structures arise from different concentrations of activators and inhibitors. A limb bud that is treated with an inhibitor will reduce the number of digits that form, as shown in Figure 24. As the concentration of the inhibitor increases, the number of digits decreases, as evident in the figures displaying five, then four, then two digits. The presence of the inhibitor alters characteristics of the system such as cell traction and motility as well as the size of the recruitment zones. These alterations lead to the failure of bifurcation events, and thus, fewer digits.

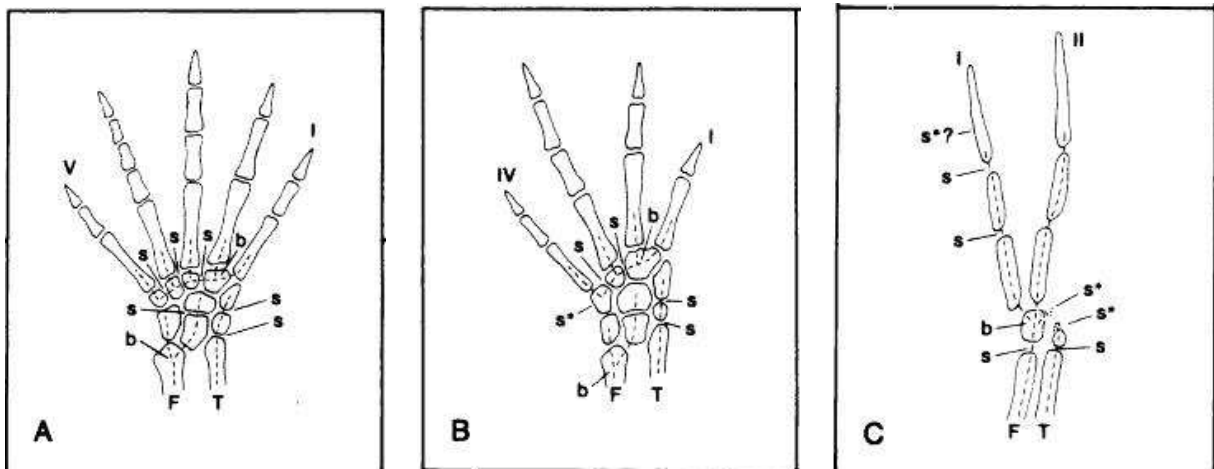


**Figure 24.** Number of digits based on inhibitor concentration [17].

### 2.3.1 Limb Geometry

There are three basic types of patterns that occur in limbs – focal condensations, branching bifurcations, and segmental bifurcations. Focal condensations result from an isolated focus, as shown in part **A** of Figure 25. They can result when the surrounding region becomes unstable from a certain balance of activation and lateral inhibition. Part **B** of the figure shows a branching bifurcation, which occurs as a result of a condensation branching into two. If the existing condensation becomes sufficiently large, its borders each attempt to define its own recruitment zone, resulting in the condensation splitting in two. The third type of pattern is a segmental bifurcation, depicted in part **C** of the figure. Segments can result from a bud splitting off the end of an existing condensation or a condensation that longitudinally divides into two smaller segments. Segmentation is similar to branching, except segmentation occurs longitudinally as opposed to laterally.



**Figure 25.** Three types of patterns occurring in limbs [17].

Several limb patterns generated from combinations of focal condensations, branching, and segmentation appear in Figure 26.

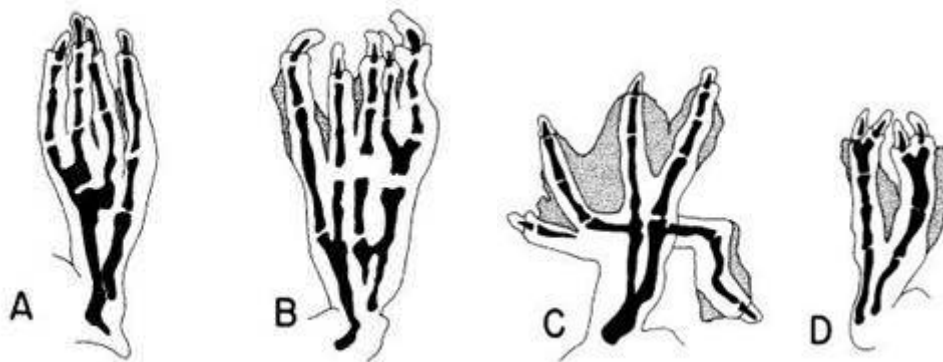


**Figure 26.** Patterns from focal condensations, branching, and segmentation [17].

### 2.3.2 Mathematical Model

As mentioned previously, the development of limbs is based on an activation-inhibition model in which cells follow a chemical gradient. An increase in the chemoattractant concentration defines the autocatalysis process, while the depletion of cells in the area surrounding a focus provides the lateral inhibition mechanism.



Below is an equation [17] for the cell density,  $n(x,t)$ .

$$\frac{\partial n}{\partial t} = M \frac{\partial^2 n}{\partial x^2} - \alpha \frac{\partial}{\partial x} n \frac{\partial c}{\partial x}$$

where  $M$  is the cell motility,  $\alpha$  is the chemotactic motility, and  $c$  is the attractant concentration. The first term on the right hand side indicates random motility, and the second term denotes chemotaxis. Thus, the equation gives the rate of change for cell density based on motility and chemotaxis.

An equation [17] for the attractant concentration  $c(x,t)$  follows.

$$\frac{\partial c}{\partial t} = D \frac{\partial^2 c}{\partial x^2} + \frac{bn}{n+h} - \mu c$$

where  $D$  is the diffusion coefficient of  $c$ ,  $b$  and  $h$  are parameters associated with the rate of secretion of chemoattractant, and  $\mu$  is the degradation rate of the chemoattractant. The first term on the right hand side denotes diffusion, the second term indicates secretion by cells, and the third term denotes the decay. Hence, the equation gives the rate of change for attractant concentration based on diffusion, secretion, and decay of the attractant.

## 2.4 Follicles and Bristles

Follicles are derived from a portion of epithelial tissue that buds, elongates, and invaginates. From the follicles emerge various skin appendages such as hair, feathers, whiskers, scales, nails, claws, horns, and glands. These useful structures have a variety of functions including temperature regulation, movement, secretion, and defense. The distribution and morphology of follicles are based on the activation-inhibition model. Several examples of the effect of activation-inhibition on follicle development are discussed below.

### 2.4.1 Distribution of Follicles

The distribution and spacing of follicles are dependent on the concentrations of activators and inhibitors. Moderate overexpression of an activator leads to an increase in follicle density. Moderate overexpression of an inhibitor results in a decrease in follicle density, i.e., enlarging of the space between follicles. This phenomenon is illustrated in Figure 27.

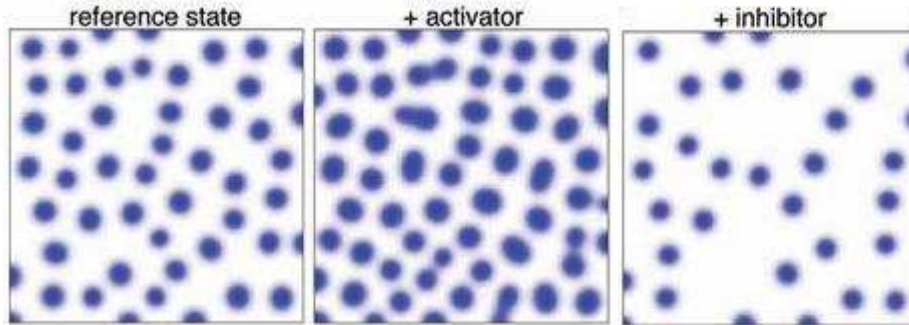


**Figure 27.** Effect of activator and inhibitor on follicle distribution in first wave [19].

Figure 28 shows the effect of activation and inhibition during a second wave of follicle induction. The larger blue circles are follicles resulting from the first induction wave, and the smaller red circles are produced during the second wave. The leftmost image shows the result from normal levels of activator and inhibitor. The effect of increased activation is displayed in the middle image. The space between the first wave follicles becomes more densely packed with second wave follicles compared to the normal case. The rightmost image shows the effect of increased inhibition. As expected, fewer second wave follicles are formed in the inter-follicle space.

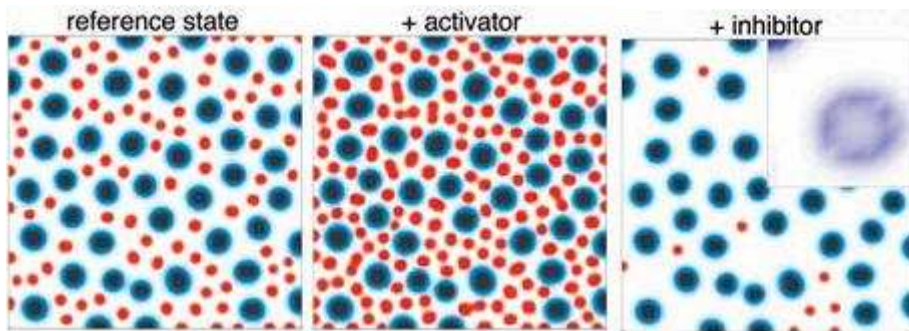


**Figure 28.** Effect of activator and inhibitor on follicle distribution in second wave [19].

Each successive wave of follicle formation causes new follicles to form between existing follicles, as evident in the previous two figures. Another view of this effect is illustrated in Figure 29. The first follicle that forms is known as a guard follicle, and it is labeled with a **1** in the figure. The follicles numbered **2** then develop from the line of tissue above the guard follicle. Follicles numbered **3** subsequently develop between the number **2** follicles. Finally, number **4** follicles develop between each of the number **2** and number **3** follicles.



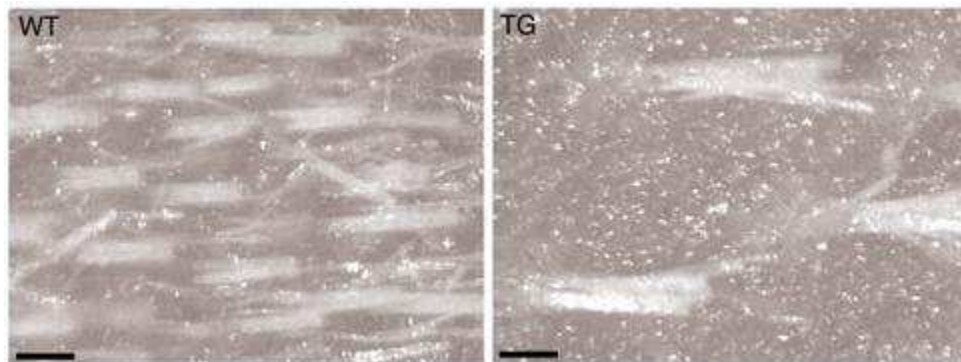
**Figure 29.** Successive stages of follicle development [19].

Figure 30 shows the effect of inhibitor concentration on hair growth of mice. The first image is the wild-type (WT) mouse, the second and third are transgenic mice with medium and strong overexpression of inhibitor respectively. There is approximately a 30% reduction of hair follicles in the medium mice. In the strong mice, there is a greater reduction of follicles, resulting in nearly hairless mice which only develop guard follicles.



**Figure 30.** Effect of inhibitor on mouse hair coat [19].

In wild-type mice, hair follicles are nearly distributed evenly, whereas in mice with an increased concentration of inhibitor, the follicles become more spread out. This effect is illustrated in Figure 31. The first panel indicates wild-type mice and the second panel represents transgenic mice.



**Figure 31.** Effect of inhibitor on distribution of mouse hair follicles [19].

Another phenomenon that occurs as a result of an increased concentration of inhibitor is that follicles frequently become clustered, whereas the follicles are separated in the normal case. Figure 32 illustrates this effect. The left panel shows the wild-type case and the right panel displays the case of transgenic mice.

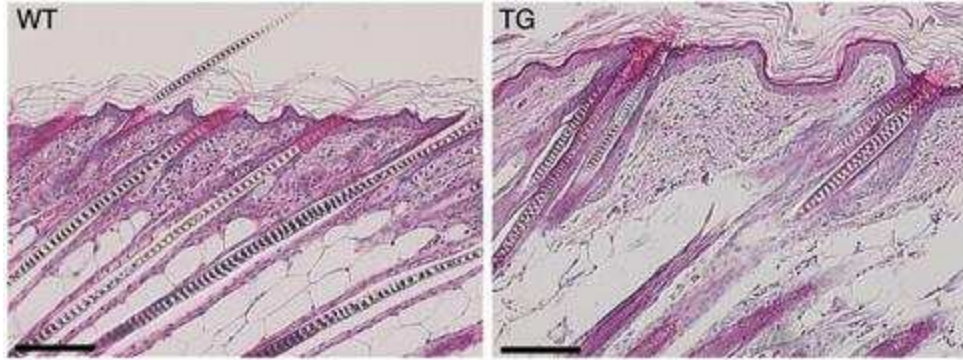


**Figure 32.** Effect of inhibitor on clustering of mouse hair follicles [19].

Varying the number of competent cells used for building follicles also affects follicle formation. As shown in Figure 33, an increase in the number of competent cells leads to an increase in the number of follicle primordia formed. Follicle buds fail to form under low cell density. As cell density is increased, cells are packed closer together until the highest density is reached, resulting in a hexagonal pattern, as indicated by the topmost square of cells in the figure.

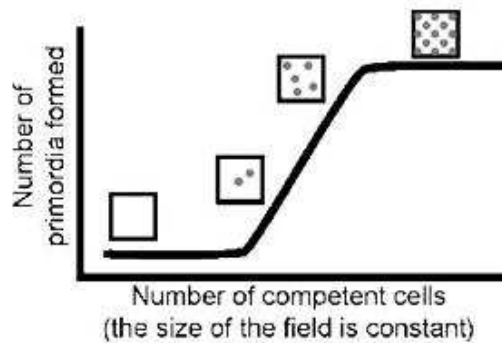


**Figure 33.** Number of follicle primordia [23].

### 2.4.2 Morphology of Follicles

The concentration of various morphogens also has an effect on the morphology of developing follicles in terms of size, shape, orientation, and structure. Figure 34 gives an example of the effect of activator-inhibitor ratio on the size of follicles. The larger the activator to inhibitor ratio, the larger the follicles, whereas a larger inhibitor to activator ratio leads to more space between follicle buds.

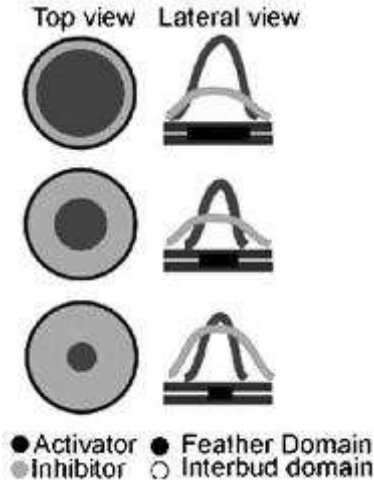


**Figure 34.** Follicle size [23].

In Figure 35, an example of the effect of activator concentration on follicle shape is illustrated. Increasing the amount of activator causes the follicle bud to stop elongating and flatten at the tip, making it plateau-shaped.



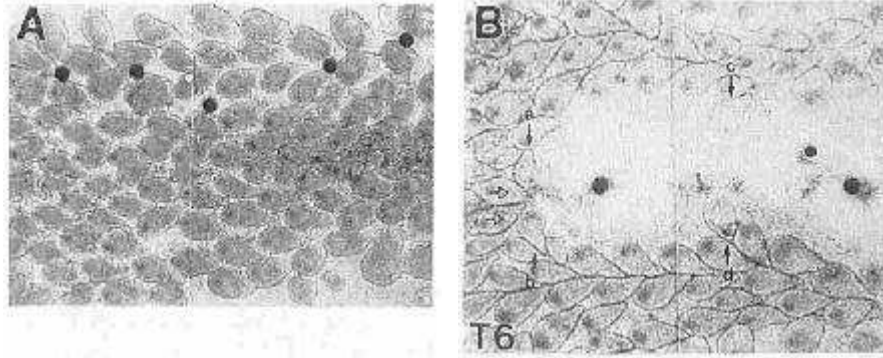
**Figure 35.** Effect of activator on follicle bud shape [23].

The effect of morphogen concentration on feather structure is shown in Figure 36. A feather is comprised of a primary branch called the rachis, secondary branches known as barbs, and tertiary branches called barbules. The leftmost image is the normal case. The middle image is a result of an increase of inhibitor concentration. The rachis is enlarged and the barbs become fused together. The rightmost image results from an overexpression of an activator. The effect is that the rachis is split and the barbs begin to branch.



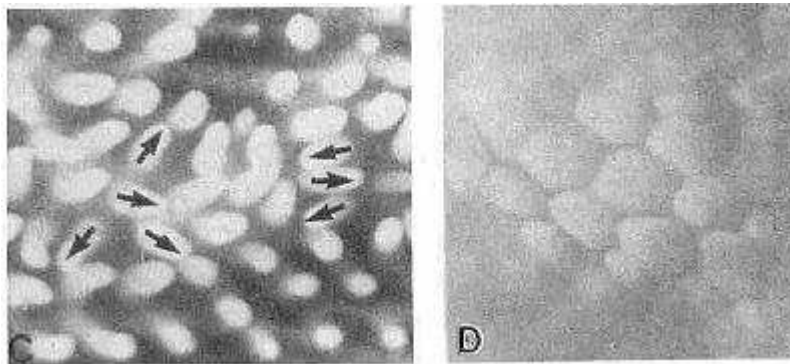
**Figure 36.** Effect of morphogen expression on feather formation [23].

Figure 37 displays the effect of morphogen concentration on the orientation of follicle structures. The left image is the control case. In the right image, inhibitors (black dots) create zones of inhibition which repel nearby buds. These zones appear in the figure as white circular regions around the black dots.



**Figure 37.** Change in orientation of follicles [3].

Concentrations of morphogens can also affect the type of structures formed. In Figure 38, increasing the concentration of a morphogen from the left image to the right image leads to feather buds becoming scale structures.



**Figure 38.** Change of feathers to scales [3].

### 2.4.3 Mathematical Model

A brief discussion of a mathematical model for skin morphogenesis follows. For a detailed presentation, the reader is referred to [5].

Skin is comprised of two layers, the epidermis and the dermis. The epidermis contains sheets of columnar cells, while the dermis consists of mesenchymal cells moving on an extracellular matrix. A fibrous basal lamina separates the epidermis and dermis. The interaction between the epidermis and dermis is an important factor in skin morphogenesis and skin pattern development. A schematic view of this interaction appears in Figure 39. The epidermal cell density is denoted by  $N$ , and the dermal cell density is indicated by  $n$ . Morphogen  $\hat{e}$  is produced by the epidermal cells and diffuses to the dermal side where it is denoted by  $e$ . Similarly, the dermal cells produce morphogen  $s$  which diffuses to the epidermal side where it is denoted by  $\hat{s}$ . The diffusion of both morphogens to the other side results in cell aggregation and the development of follicle primordia.

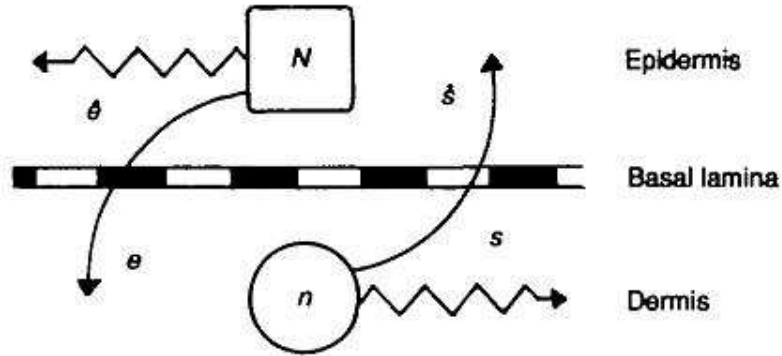


**Figure 39.** Interaction between epidermis and dermis [5].

The mathematical model [5] consists of differential equations to describe the rate of change of the various morphogen concentrations and cell densities. First, define

- $\hat{e}(x,t)$  = epidermal concentration of morphogen produced in epidermis at position  $x$  and time  $t$ ,
- $s(x,t)$  = dermal concentration of morphogen produced in dermis,
- $e(x,t)$  = dermal concentration of morphogen received from epidermis,
- $\hat{s}(x,t)$  = epidermal concentration of morphogen received from dermis

The conceptual equations describing the chemical interactions are as follows:

$$\frac{\partial \hat{e}}{\partial t} = \text{diffusion of } \hat{e} + \text{production of } \hat{s} - \text{dermal signal} - \text{degradation of } \hat{e}$$

$$\frac{\partial s}{\partial t} = \text{diffusion of } s + \text{secretion of } e - \text{epidermal signal} - \text{degradation of } s$$

$$\frac{\partial e}{\partial t} = \text{diffusion of } e + \text{dermal signal} - \text{metabolism of } e$$

$$\frac{\partial \hat{s}}{\partial t} = \text{diffusion of } \hat{s} + \text{epidermal signal} - \text{metabolism of } \hat{s}$$

The conceptual equations giving the rates of change of cell densities are

$$\frac{\partial N}{\partial t} = \text{convection}$$

$$\frac{\partial n}{\partial t} = \text{diffusion of } e - \text{chemotaxis of } e + \text{mitosis}$$

Variations of the parameters of the system will lead to the development of different skin patterns. For example, one set of parameters may produce a stripe pattern, whereas a different set of parameters may generate a pattern of spots.

#### 2.4.4 Formation of Bristles

Meinhardt's reaction-diffusion model can be used to explain the formation of bristles and follicles. Bristles form where activation peaks occur in the epithelial tissue. These peaks are surrounded by a zone of inhibition brought about by a morphogen such as a growth hormone. As cells divide and the tissue expands, the peaks become more spread out. The next wave of activation peaks develop between existing peaks at a certain distance away, where the inhibition signal is lower. Figure 40 illustrates the formation of activation peaks on a 3D surface.

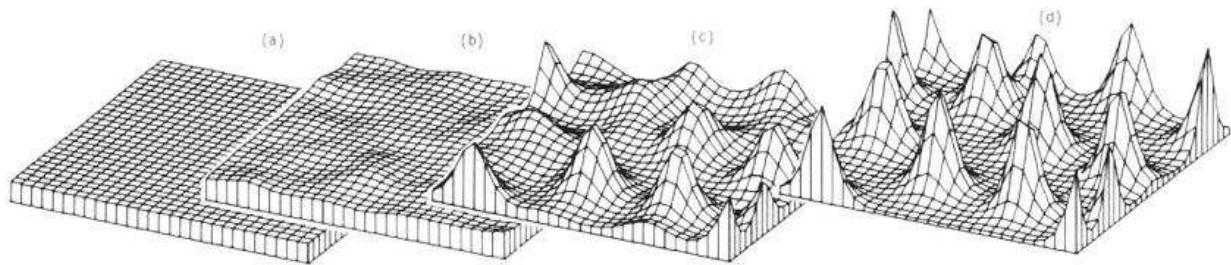


**Figure 40.** Formation of activation peaks [11].

In Figure 41a, the distribution of new activation peaks among old peaks is shown. The top image shows the configuration of the old peaks. The tissue grows, causing the peaks to spread out as evident in the bottom image. The new peaks form between the old peaks and they are denoted by the x's in the image.

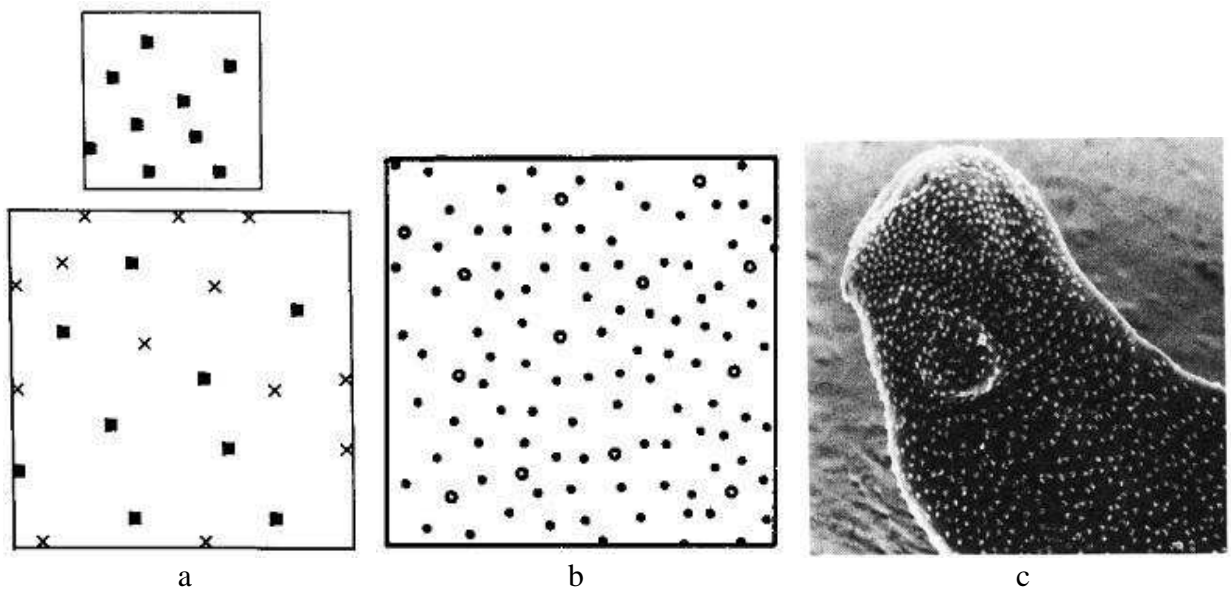


**Figure 41.** Formation of bristles and hairs [11].



Bristles on insects and other animals only form during the first four larval stages. In the fifth stage, hairs instead of bristles develop. At this point, the most recently formed activation peaks are significantly lower than their predecessors. This may well function as a signal that turns off bristle production and turns on hair production. This phenomenon is illustrated in Figure 41b. The open dots denote bristles, which have become more spread out since they were the first to develop. The hairs are denoted by the solid dots, which subsequently fill in the space between the previously formed bristles. Figure 41c gives an image of a cilia pattern on *Xenopus*.

## 2.5 Sheets and Layers

Tissues composed of sheets and layers are useful structures for secretion, containing glands, or serving as a protective covering. An example of constructing sheets of cells is presented, followed by a discussion of the development of convolutions in the cerebral cortex, which is followed by a brief example of the effect of growth rate on the geometry of sheet structures.

### 2.5.1 Sheets of Cell Aggregates

Cellular sheets can be constructed from aggregates of cells. These sheets can be used for skin or the outer layer of organs. Figure 42 shows an example of forming a sheet of cells. The sheets consist of 25 cell aggregates, each composed of 925 cells. The initial sheet pattern in image **a** is hexagonal while the image in **b** assumes a square lattice structure. The aggregates eventually fuse together to form a continuous sheet, as shown in images **c** and **d**. The sheet structures that form are dependent on interactions between cells and cell-matrix interactions. The images in **e-h** are formed using a different cell type, thus resulting in slightly different configurations.

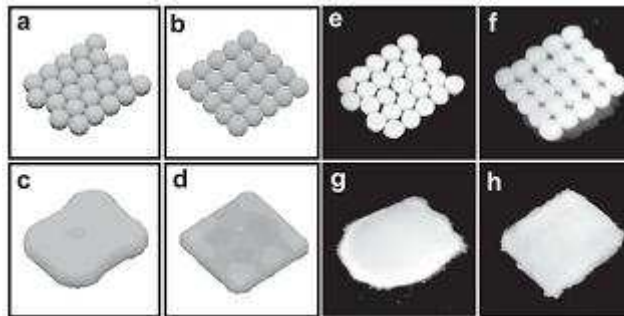


**Figure 42.** Formation of sheets from cell aggregates [14].

### 2.5.2 Cerebral Cortex Convolutions

Convolutions are folds that exist in the cortical layer. The cortex is modeled as a circular structure that contains fibers representing glia and axons that pull in a radial direction. The development of convolutions is largely dependent on mechanical factors, such as the elasticity and plasticity of the fibers and cortex, and the growth of the cortex itself [21]. Elasticity is a measure of flexibility, that is, the ability to restore the initial configuration upon deformation. Plasticity refers to the permanent modification of a structure following a strong or continuous force. A geometrical model and mathematical equations for the system can be found in [21].

Primary convolutions first develop, then secondary and tertiary convolutions, with each successive wave shallower.

### 2.5.2.1 Formation of Cortex Convolutions

There are three stages involved in the formation of convolutions: symmetric growth, development, and accommodation, as illustrated in Figure 43. The radial elements have been omitted in order to simplify the figure, however, they can be imagined as spokes of a wheel. The first stage consists of symmetric growth where the cortex structure expands in a symmetric manner. No convolutions are formed at this point. In stage II, convolutions begin to develop. Stage III involves the accommodation of the convolutions into the cortical layer. At this stage, some convolutions may fuse together, as shown by the convolutions labeled **a** and **b** merging into one convolution labeled **ab**. The numbers at the bottom of the figure denote the iteration number in the simulation.

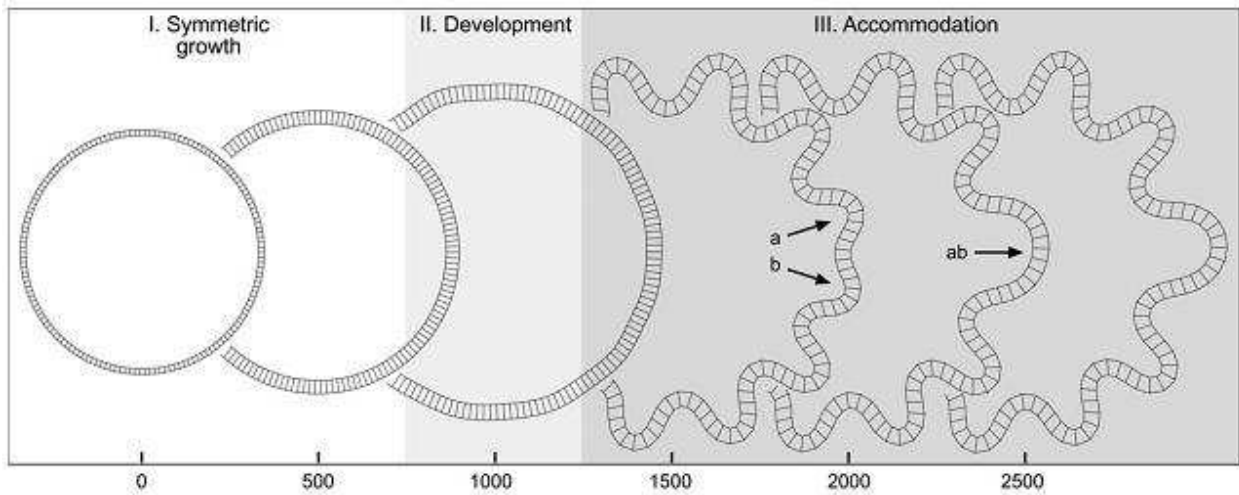


**Figure 43.** Formation of cortex convolutions [21].

There are three types of asymmetry that trigger the formation of convolutions: geometric asymmetries, mechanical asymmetries, and growth asymmetries. Each of these asymmetries is discussed in turn.

### 2.5.2.2 Geometric Asymmetries

One type of geometric asymmetry is a perturbation of a single point, as indicated by the large arrow in Figure 44. This perturbation leads to the formation of a primary convolution at the perturbation point, which then triggers several waves of convolutions to form towards the top and bottom of the cortex. The primary convolution is the deepest, and each successive convolution formed thereafter is shallower, as evident in the figure.

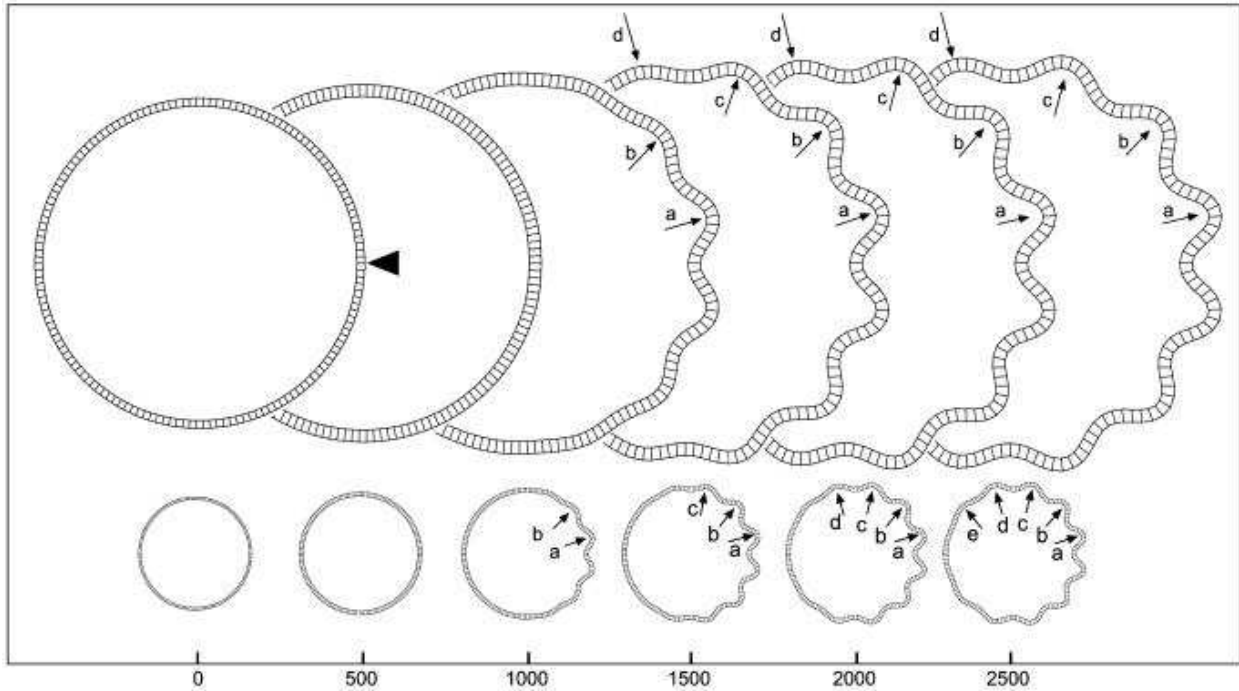


**Figure 44.** Effect of perturbation on convolution formation [21].

Another type of geometrical asymmetry is modification of the initial shape of the cortex. Instead of using a circular configuration, an elliptical shape is used in Figure 45. In this case, the convolutions begin at the top and bottom of the cortex, and spread towards the side, with each successive convolution becoming shallower.

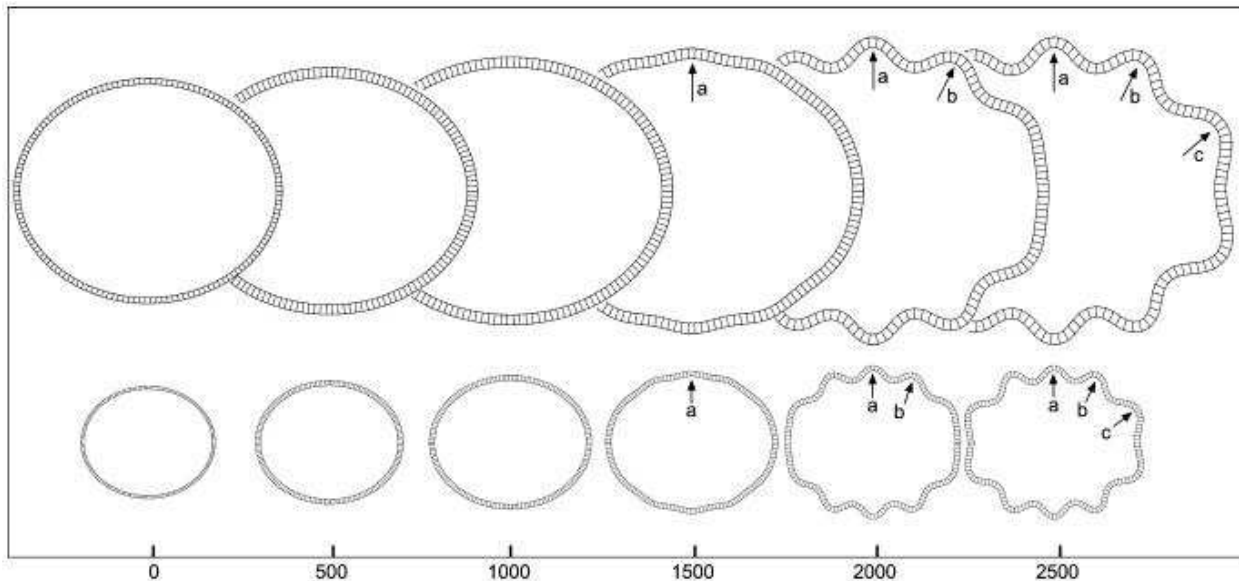


**Figure 45.** Effect of ellipse shape on convolution formation [21].

### 2.5.2.3 Mechanical Asymmetries

Two types of mechanical asymmetries discussed here are steps and gradients in the elastic constant of the cortex. Figure 46 shows the simulation from using steps in the elastic constant. The darker region of the cortex is more elastic. The primary convolution forms in the middle where the darker and lighter halves meet. This induces a wave of convolutions to propagate towards the top and bottom of the cortex. The convolutions are notably deeper in the more elastic half.

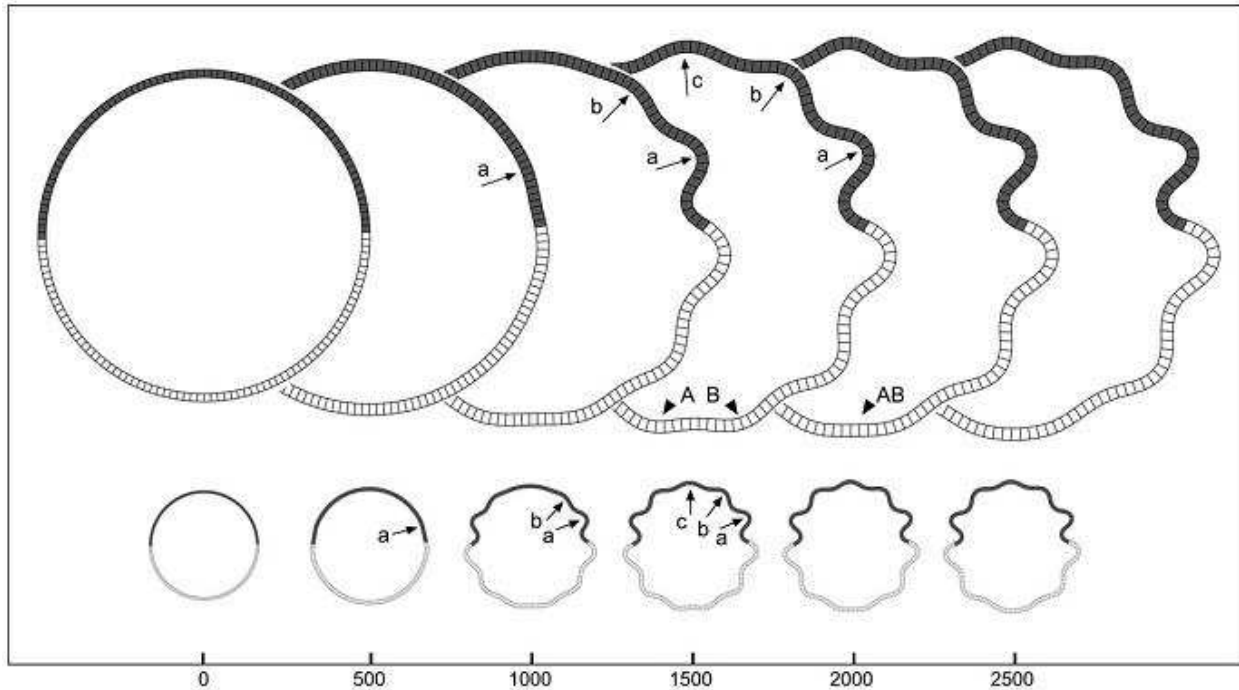


**Figure 46.** Effect of mechanic step on convolution formation [21].

Figure 47 shows the result of introducing a gradient in the elastic constant. Convolutions develop simultaneously at several points and they are deeper in the more elastic half of the cortex.

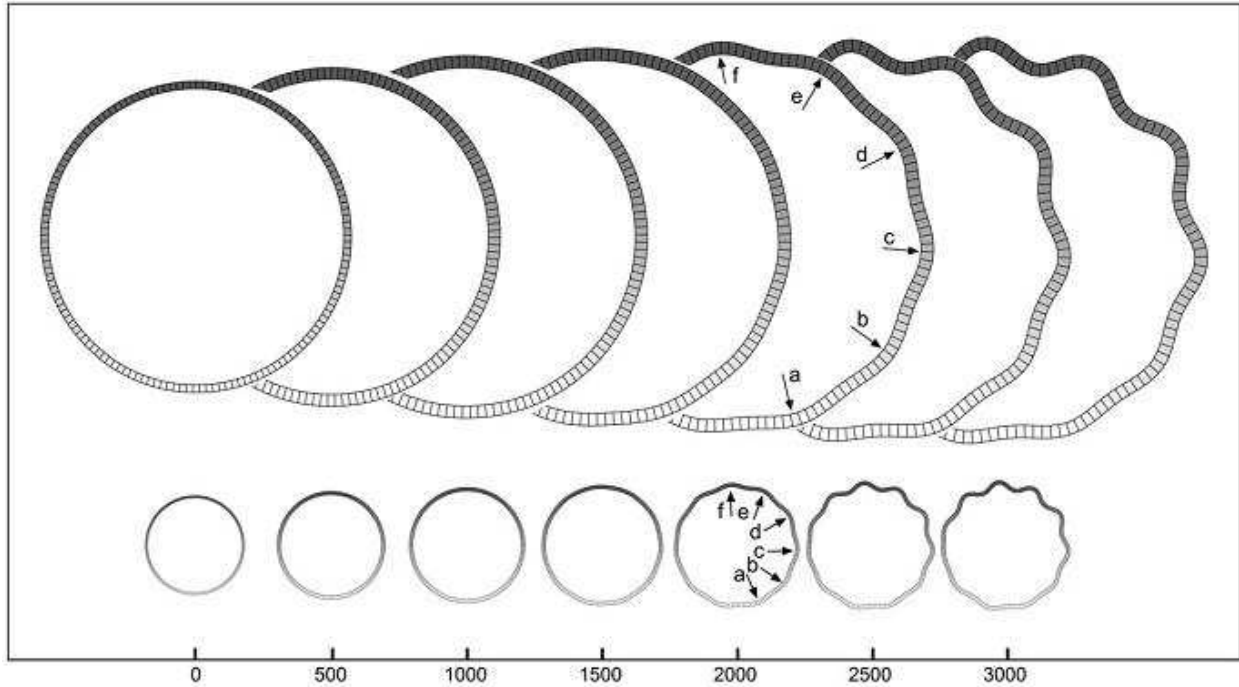


**Figure 47.** Effect of mechanic gradient on convolution formation [21].

#### 2.5.2.4 Growth Asymmetries

Similar to the mechanical asymmetry cases, applying steps and gradients to the growth of the cortex leads to the development of convolutions. The steps and gradients are introduced in the carrying capacity parameter of the logistic-growth function. Figure 48 shows the effect of growth step on convolution development. There is larger growth at the top half of the cortex, and smaller growth at the bottom. The primary convolution forms at the border of the top and bottom halves, and this induces successive waves of convolutions to develop towards the top and bottom of the cortex which are progressively shallower. The convolutions are more pronounced in the area containing more growth, i.e., the top half.

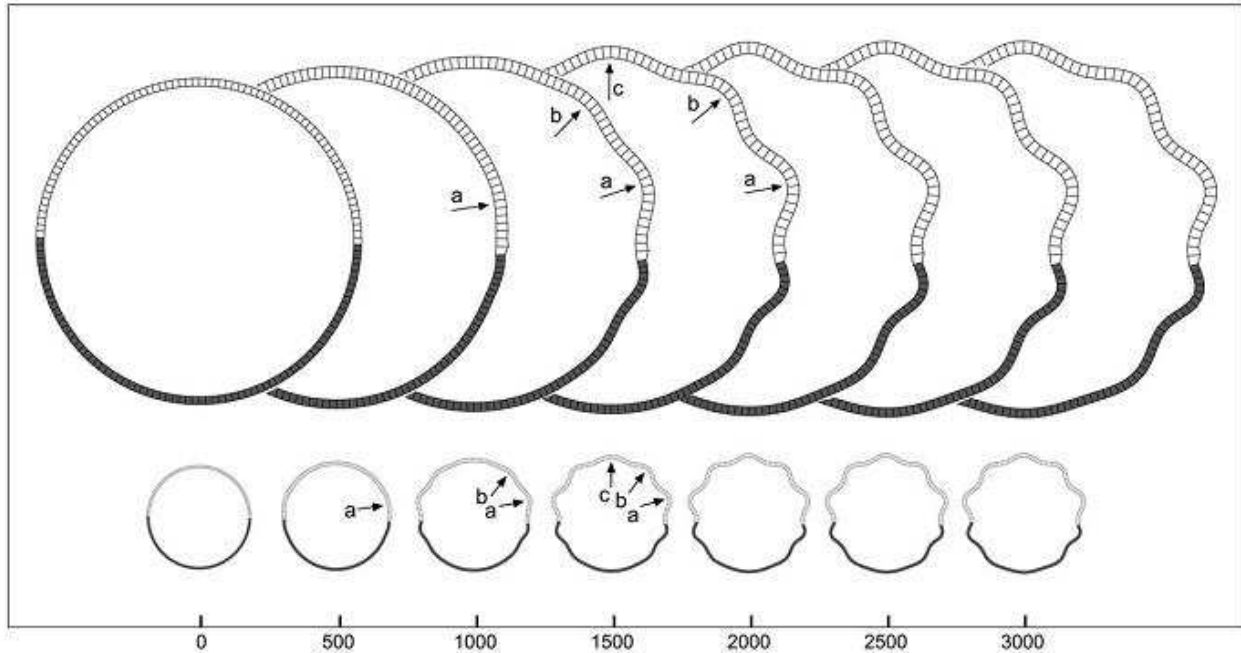


**Figure 48.** Effect of growth step on convolution formation [21].

Figure 49 shows the result of applying gradient to the carrying capacity of the cortex. The convolutions are formed simultaneously and they become deeper as they move from the region of less growth to the region of more growth.

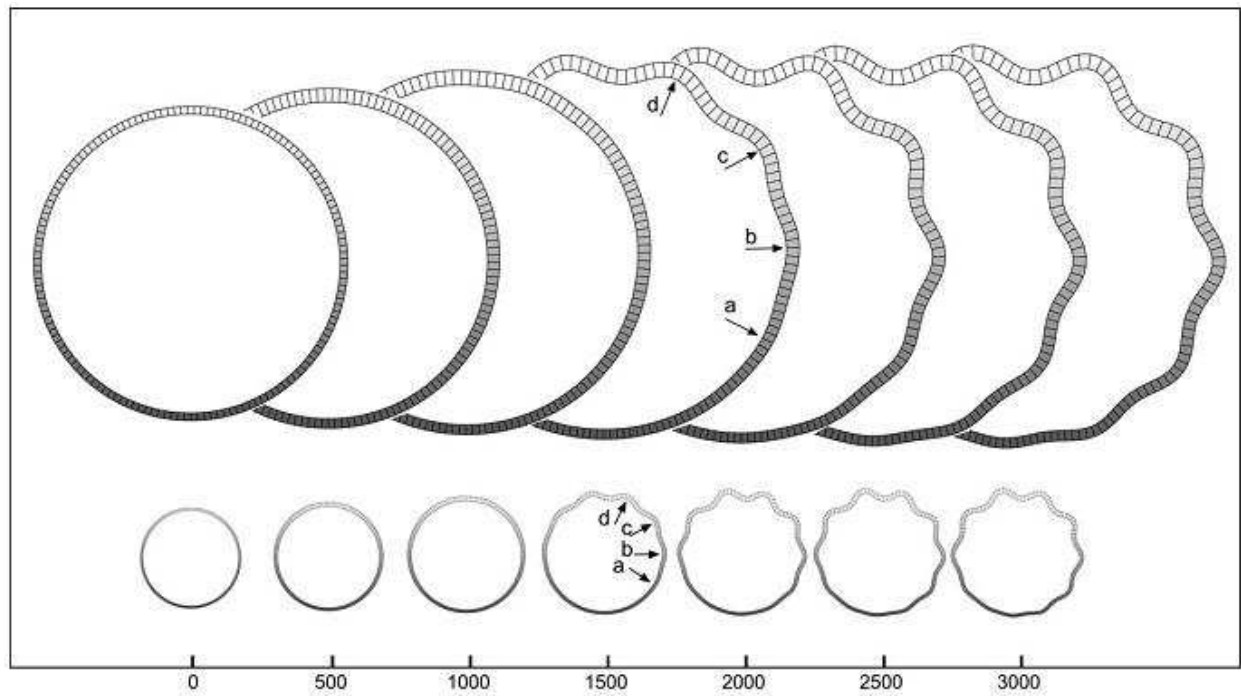


**Figure 49.** Effect of growth gradient on convolution formation [21].

### 2.5.3 Effect of Growth Rate on Geometry of Structures

The shape of a given structure can be influenced by the varying rate of growth in different areas of the structure [4]. This phenomenon can be seen in Figure 50. In **a**, the rate of growth increases from left to right. The cells of the faster-growing right end begin to rotate relative to each other, resulting in a curved shape at that end. In **b**, the growth rate is higher at the edges than it is in the center, thus, the edges bend and the structure forms a wavy edge. This phenomenon is also present in *cincinnata* mutants [4], where the leaves show significant rippling at the edges, resulting from a delay in the arrest of growth at the leaf's edges.

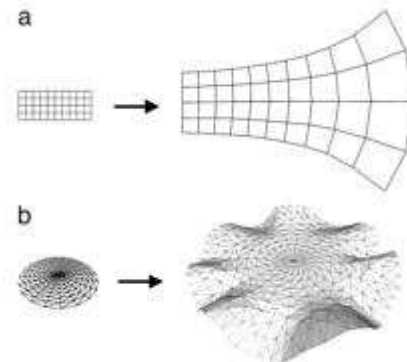


**Figure 50.** Growth rate's effect on geometry [4].

## 2.6 Segments and Somites

In the developing vertebrate embryo, segments of cells form along the anterior-posterior axis. These undifferentiated segments eventually become somites, which are precursors to muscle, skeletal, and skin components of the organism. Somites are repeating, periodic structures that occur in pairs straddling the notochord. The formation of somites is largely based on cell rearrangements and changes in cell shape. Somites become rounded as they separate from each other. Somite borders are formed either by fissures or by a ball and socket separation of somites. Figure 51 illustrates somite pattern formation in a developing embryo. The somites labeled **s0** are newly developing somites, and development progresses in the anterior to posterior direction. The neural tube is denoted by **nt**, and **PSM** indicates the presomatic mesoderm, from which somites develop.

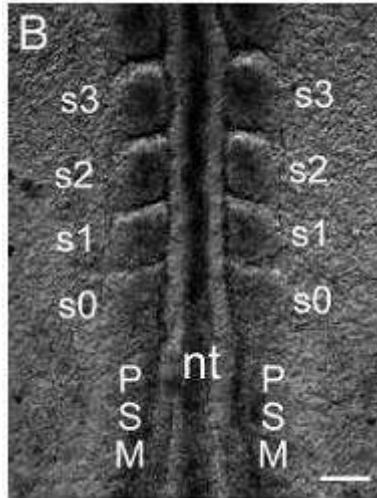


**Figure 51.** Formation of somites in embryo [10].

Several models have been developed in attempt to describe the process of somite formation. The three models discussed here are more commonly studied: the clock and wavefront model, the cell cycle model, and the reaction-diffusion model. There are numerous other models that have recently been proposed including the cell-cell adhesion model [1] and the oscillator model [13]. A more detailed listing of models is given in [10].

### 2.6.1 Clock and Wavefront Model

The clock and wavefront model is based on two parameters, a cellular oscillator (clock), which controls when somite borders form, and a wavefront, which controls where somite borders form [10]. The clock determines when cells undergo major changes in adhesive and migratory properties in preparation to form somites. Cells follow a gradient of fibroblast growth factor (FGF) until the FGF signal reaches a limit known as the determination front, the point at which cells become committed to form somites. The clock controls the wavefront by periodically enabling its propagation down the axis. This process is illustrated in Figure 52. Somites form in the anterior (left) to posterior (right) direction. The PSM is initially homogeneous and the passing wavefront triggers several cells to form segments, which are somite precursors.

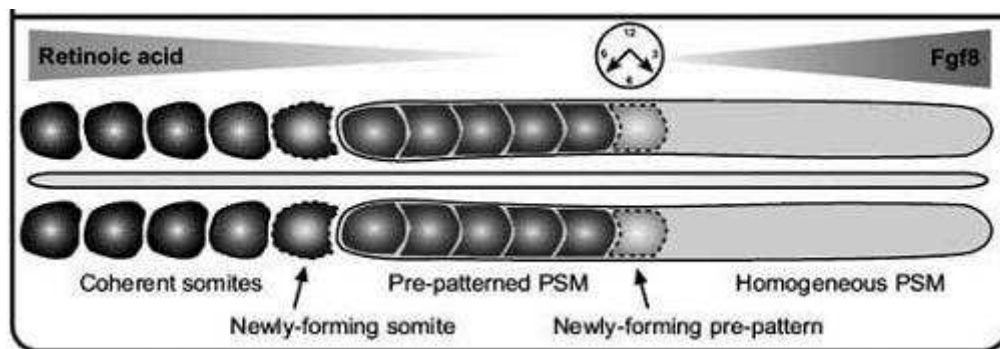


**Figure 52.** The clock and wavefront model of somite formation [10].



The clock and wavefront also determine the size of the developing somites. Decreasing the frequency of clock oscillations and accelerating the passing wavefront will both increase somite size [2].

The wavefront is determined by the interaction between FGF and retinoic acid which act in a negative feedback loop with one another. This feedback loop controls the FGF signal gradient which in turn regulates the wavefront. The clock is determined by the interaction of an mRNA and its protein product which causes a delay by suppressing its own gene expression. Mathematical equations for the clock and wavefront model can be found in [10].

### 2.6.2 Cell Cycle Model

The cell cycle model associates the cell cycle with somite formation. It assumes a level of cell synchronicity between cells in the PSM. The process works in the anterior to posterior direction, with anterior cells being more mature. Figure 53 illustrates the process of segmentation given by the cell cycle model. The model defines two points in the PSM cell cycle,  $P_1$  and  $P_2$ , which are 90 minutes apart. Cells that have not reached  $P_1$  in their cell cycle are not yet ready for segmentation. These cells are located posterior to the forming somite. Between  $P_1$  and  $P_2$  is when cells gain competency for segmentation. Because of synchronicity, some of the cells that will form a somite together reach  $P_2$  before the others in that future somite. These cells produce a signal to which the other cells between  $P_1$  and  $P_2$  in their cycle respond by undergoing cell changes to prepare for somite formation. Beyond  $P_2$ , cells are considered somitic. A mathematical model of the cell cycle process is presented in [2].

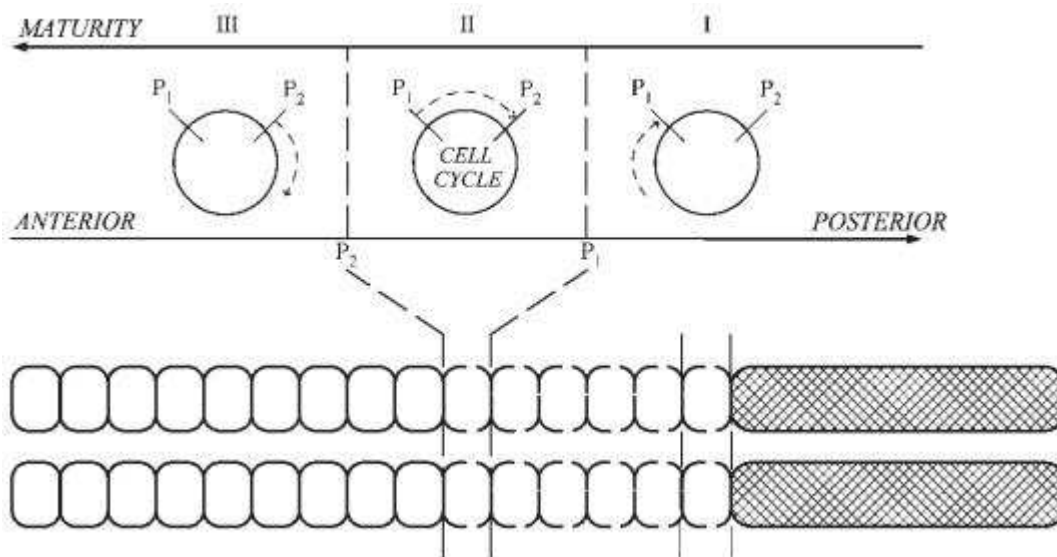


**Figure 53.** The cell cycle model of somite formation [2].

In Figure 54, the effect of applying the morphogen FGF is shown. The bottom rows correspond to a control embryo and the top rows correspond to an embryo to which FGF is applied. The application of FGF causes some of the somites to be smaller than normal, these being followed by a larger than normal somite. The right side of the figure illustrates the effect of increasing the strength of the FGF morphogen. Unusually small and large somites are formed as in the

previous case; in addition, an extra somite is developed. Varying the concentration of the FGF morphogen can produce different numbers and sizes of somites.

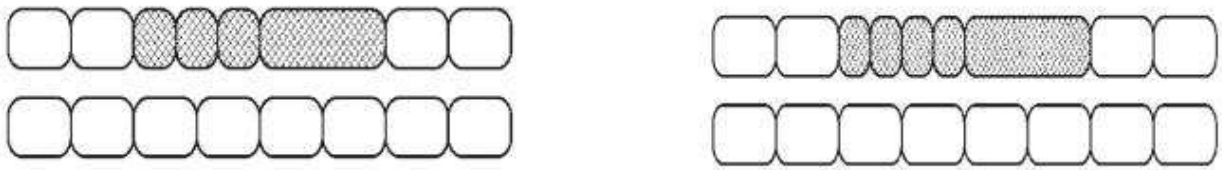


**Figure 54.** Effect of applying morphogen to forming somites [2].

### 2.6.3 Reaction-Diffusion Model

The reaction-diffusion model for the formation of somites was developed by Meinhardt [11]. A cell can either be in state **a** (anterior) or state **p** (posterior). Cells in state **a** produce substance X and cells in state **p** produce substance Y. For cells in state **a**, the ability to produce X is turned on, and similar for cells in **p** producing Y. The two states inhibit one another at the local level and activate each other over a distance. Cells alternate between states until they become stable. Thus, a pattern of ...**apap**... is produced in the anterior to posterior direction. A pair **ap** represents a segment with an anterior and a posterior half, the transition between the two indicating a change of specification of the segment. There are two possibilities for controlling a cell's change in state. One possibility is the existence of a morphogen gradient and the other is the growth of the domain in the posterior direction [2].

## 3 Conclusions

In this review, the formation of several different useful and interesting biological structures was discussed. Many of the mathematical models behind their development were analyzed, such as the reaction-diffusion model and the clock and wavefront model. Acquiring an understanding of the underlying processes driving the development of biological structures will provide substantial insight into the creation of innovative artificial structures for useful purposes. The ability to build such structures from the bottom up will lead the field of nanotechnology into a direction of unprecedented sophistication.

## References

- [1] Armstrong, NJ. et al. A Continuum Approach to Modeling Cell-Cell Adhesion, *Journal of Theoretical Biology*, Vol. 243, pp. 98-113, 2006. **Referred to by the Segment to Somite paper in [10].**
- [2] Baker, R. et al. Formation of Vertebral Precursors: Past Models and Future Predictions, *Journal of Theoretical Medicine*, Vol. 5, No. 1, pp. 23-35, March 2003. **Contains discussion of three models for somitogenesis: clock and wavefront, cell-cycle, and reaction-diffusion. Contains schematic diagram and mathematical equations for cell-cycle model.**

[3] Chuong, C., WidELITZ, R., Jiang, T. Adhesion Molecules and Homeoproteins in the Phenotypic Determination of Skin Appendages, *Journal of Investigative Dermatology*, Vol. 101, No. 1, Supplement, July 1993. **Contains model for feather development, mostly from a genetics point of view. Contains several images resulting from changes in morphogen concentration.**

[4] Coen, E., Rolland-Lagan, A-G., Matthews, M., Bangham, J. A., Prusinkiewicz, P. The Genetics of Geometry, *PNAS*, Vol. 101, No. 14, pp. 4728-4735, April 2004. **Contains examples of the effect of growth properties on the shape and geometry of developing structures.**

[5] Cruywagen, G., Maini, P. K. Sequential Pattern Formation in a Model for Skin Morphogenesis, *Journal of Mathematics Applied in Medicine & Biology*, Vol. 9, pp. 227-248, 1992. **Contains very detailed mathematical model (numerous differential equations) for follicle development.**

[6] Gottlieb, M. E. The VT Model: A Deterministic Model of Angiogenesis, *IEEE Transactions on Biomedical Engineering*, 1993. **Referred to by the paper on visualizing biological structures in [18].**

[7] Hogan, B., Kolodziej, P. Molecular Mechanisms of Tubulogenesis (Review), *Nature Reviews*, Vol. 3, pp. 513-523, July 2002. **Contains discussion and schematic diagrams of the mechanics of tube development from a genetics perspective. Also references reviews on kidney and pancreas organogenesis.**

[8] Kaandorp, J. Modeling Growth Forms of Sponges with Fractal Techniques, *Fractals and Chaos*, Springer-Verlag, 1991. **Referred to by the paper on visualizing biological structures in [18].**

[9] Kondo, S. The Reaction-Diffusion System: A Mechanism for Autonomous Pattern Formation in the Animal Skin (Review), *Genes To Cells*, Vol. 7, pp. 535-541, 2002. **Contains brief overview of reaction-diffusion model and examples of stripes and spots patterns in animal skin.**

[10] Kulesa, P. et al. From Segment to Somite: Segmentation to Epithelialization Analyzed Within Quantitative Frameworks (Review), *Developmental Dynamics*, Vol. 236, pp. 1392-1402, 2007. **Contains models for segments forming somites, in particular the clock and wavefront model, including a schematic diagram and mathematical equations. Also contains a table of many examples of models for somite formation.**

[11] Meinhardt, H. *Models of Biological Pattern Formation*, London: Academic Press, 1982. **Contains details of mathematical model of reaction-diffusion, and many examples of the development of structures, including bristles.**

[12] Metzger, R. J., Klein, O. D., Martin, G. R., Krasnow, M. A. The Branching Programme of Mouse Lung Development, *Nature*, Vol. 453, pp. 745-750, 2008. **Contains a discussion of**

**several types of branching modes applied to mouse lung development.**

[13] Monk, NA. Oscillatory Expression of Hes1, p53 and NF-kappaB Driven By Transcriptional Time Delays, *Current Biology*, Vol. 13, pp. 1409-1413, 2003. **Referred to by the Segment to Somite paper in [10].**

[14] Neagu, A. et al. Role of Physical Mechanisms in Biological Self-Organization (Review), *Physical Review*, 95, 178104, 2005. **Contains a model for developing general sheets and tubes from aggregates of cells.**

[15] Nelson, T.R., Manchester, D. K. Modeling of Lung Morphogenesis Using Fractal Geometries, *IEEE Transactions on Medical Imaging*, Vol. 7, No. 4, pp. 321-327, Dec. 1988. **Contains a fractal model for lung airway development, including mathematical equations. Shows several diagrams of changes resulting from varying a parameter.**

[16] Odell, G. M., Oster, G., Alberch, P., Burnside, B. The Mechanical Basis of Morphogenesis, *Developmental Biology*, Vol. 85, No. 2, pp. 446-462, 1981. **Classic paper that describes the mathematical model of epithelial folding and invagination.**

[17] Oster, G. et al. Evolution and Morphogenetic Rules: The Shape of the Vertebrate Limb in Ontogeny and Phylogeny, *Evolution*, Vol. 42, No. 5, pp. 862-884, 1988. **Contains analysis of limb development from an evolution point of view. Contains several images and mathematical appendices.**

[18] Prusinkiewicz, P. Modeling and Visualization of Biological Structures, *Proceedings of Graphics Interface*, pp. 128-137, May 1993. **Contains brief overview of various mathematical models of pattern generation including reaction-diffusion, cellular automata, space expansion, and L-systems. Contains diagrams of different branching structures generated, in addition to realistic images from computer simulations.**

[19] Sick, S. et al. WNT and DKK Determine Hair Follicle Spacing Through a Reaction-Diffusion Mechanism (Report), *Science*, Vol. 314, pp. 1447-1450, Dec. 2006. **Contains reaction-diffusion model for follicle development and distribution. Contains numerous images showing results from different overexpressions of activator/inhibitor.**

[20] Takaki, R. Can Morphogenesis Be Understood in Terms of Physical Rules?, *Journal of Bioscience*, Vol. 30, No. 1, pp. 87-92, Feb. 2005. **Contains brief overview of mathematical equations or algorithms for generating the lung airway, liver blood vessels, and liver capillary network. Contains images from computer simulations.**

[21] Toro, R. and Burnod, Y. A Morphogenetic Model for the Development of Cortical Convolutions, *Cerebral Cortex*, Vol. 15, pp. 1900-1913, 2005. **Contains geometric and mechanical model for the development of cortex convolutions. Shows examples of asymmetries that produce convolutions, including several diagrams.**

[22] Ulam, S. On Some Mathematical Properties Connected with Patterns of Growth of Figures, *Proceedings of Symposia on Applied Mathematics*, Vol. 14, pp. 215-224, 1962. **Referred to by the paper on visualizing biological structures in [18].**

[23] Widelitz, R. et al. Molecular Biology of Feather Morphogenesis: A Testable Model for Evo-Devo Research, *Journal of Experimental Zoology (Mol Dev Evol)*, Vol. 298B, pp. 109-122, 2003. **Contains analysis of feather life cycle, feather follicle formation, and actual feather development, mostly from a genetics perspective.**

## Appendix – Reaction-Diffusion (RD) Model

Two morphogens, known as activator and inhibitor, diffuse throughout a medium at different rates. The activator triggers the production of itself and an inhibitor, which inhibits the production of the activator. Thus, the activator engages in an autocatalytic process while the inhibitor provides negative feedback to the system. The coupling of short range activation and long range inhibition leads to periodic waves of activation and inhibition. When the inhibitor diffuses faster than its activator, interesting patterns can emerge. Three important aspects of a reaction-diffusion system are that it is autonomous, the formed patterns are stable, and a pattern can restore its original configuration upon perturbation [9]. Patterns generated by a reaction-diffusion system include patterns of stripes or spots on animal skin, as shown in Figure 55. The stripes on the zebra (left image) exhibit regional variation, whereas the stripe pattern on the catfish (right image) is uniform throughout.



**Figure 55.** Stripe patterns in zebra and catfish [9].

Figure 56 gives several examples of patterns generated by varying a parameter in the reaction-diffusion equations. As the parameter is varied, different structures are developed. Smaller values of the parameter lead to stripes (left), medium values result in maze-like patterns (middle), and larger parameter values generate isolated spots (right).



**Figure 56.** Various patterns from different parameter values in RD equations [9].

Below are given equations for the activator and inhibitor respectively [11]:

$$\frac{\partial a}{\partial t} = \frac{\rho a^2}{h} - \mu a + D_a \frac{\partial^2 a}{\partial x^2}$$

$$\frac{\partial h}{\partial t} = \rho' a^2 - \nu h + D_h \frac{\partial^2 h}{\partial x^2}$$

The first equation gives the rate of change of the activator concentration, and the second equation gives the rate of change of the concentration of the inhibitor. The first term of the activator equation denotes the present concentration of the activator, which is inversely proportional to the concentration of the inhibitor. The second term indicates the decay of the activator. The third term gives the rate of diffusion of the activator, where  $D_a$  is a diffusion constant. In the inhibitor equation, the first term gives the concentration of the activator rather than that of the inhibitor since the inhibitor's presence is dependent on the activator's concentration. The second term denotes the decay of the inhibitor. The rate of diffusion of the inhibitor is indicated by the third term of the equation, where  $D_h$  is a diffusion constant. Details of the mathematical model can be found in Meinhardt's text [11].